Nonlinearity Compensation in Digital Radio Systems

Giovanni Lazzarin, Silvano Pupolin, *Senior Member, IEEE* and Augusto Sarti, *Member, IEEE*

Abstract—**Digital radio links with bandlimited pulses exhibit a severe performance degradation when the transmitter high power amplifier operates near saturation. To cope with the increase of nonlinear intersymbol interference due to the amplifier nonlinearities, a discrete-time Volterra system can be used to process the transmitted data.**

We present an efficient technique for implementing adaptive data predistorters with memory based on a discrete-time Volterra system composed of digital linear filters and memoryless nonlinear devices working at the symbol rate. Third- and fifth-order structures are proposed and a system performance evaluation is presented for several realistic situations.

I. INTRODUCTION

IN order to allow the maximum exploitation of the RF spectrum, the current trend in the design of digital radio systems is to increase the spectrum efficiency by using high capacity modulation formats such as multilevel quadrature amplitude modulation (QAM) with bandlimited pulses to reduce the adjacent channel interference (ACI). On the other hand, the need for good power efficiency forces the drawing of the transmitter high power amplifier (HPA) to near saturation, where the nonlinear distortion, acting on a bandlimited pulse stream, gives rise to some unwanted effects, such as: i) the increase of the intersymbol interference (ISI) (the detector receives a warped constellation of clusters), and ii) the increase of the ACI due to a widening of the transmitted signal spectrum. The severity of both these effects increases as the size of the alphabet increases.

When the HPA nonlinearity becomes a significant source of impairment a number of questions arise. For instance: what special circuitry should be used to compensate for the nonlinearity? What is the best design for the filter shaping? What are the best constellations? In recent years many authors have given some partial solutions to these problems. The proposed methods may be divided into two main classes, those operating on the transmitter side (TX), and those operating on the receiver side (RX). The optimal solution among the RX-techniques is the maximum likelihood sequence estimation (MLSE) technique proposed by Mesiya, Mc Lane and Campbell [1] and also by Van Etten and Van Vugt [2]. Other suboptimal methods are nonlinear equalization, as proposed by Falconer [3] and Benedetto and Biglieri [4], and the adaptive cancellation of the nonlinear ISI, due to Biglieri, Gersho, Gitlin and Lim [5]. The main limitation of these techniques, besides the fact that they cannot do anything to avoid spectrum widening, is their complexity.

The TX-techniques perform a transformation of the HPA input signal by using a nonlinear device in order to improve the linearity of the overall link. This operation is very simple for a memoryless end-to-end link because, in this case, the compensator becomes a nonlinear digital mapper that warps the source constellation in order to reshape the detected constellation as desired. The pioneering paper by Saleh and Salz [6], in which this technique was proposed for rectangular pulses, has been followed by others [7-8] for bandlimited pulseshaping. However, with bandlimited pulses, the received signal exhibits a "clustering" effect, due to the nonlinear ISI, while a nonlinear mapper can only correct the average positions of the individual clusters without reducing their variance. Therefore, the performance improvement in the case of band-limited pulses is smaller than with time-limited pulses and worsens as the size of the alphabet increases.

Another TX-technique able to cope with the increase of nonlinear ISI consists of the insertion of an appropriate analog device (analog predistorter) [9,10] before the amplifier that is to be linearized.

Recently proposed solutions involve processing of the data sequence using a nonlinear filter. The developed techniques are based on: i) discrete-time Volterra system, ii) nonlinear data interpolation and iii) appropriate coding of the data message. The first was addressed in its general theoretical solution by Biglieri et al. [11], and further by others [12-13]. The second was proposed by Karam and Sari [14-15], while the last is, as of yet, a nearly unexplored technique.

In this paper we set up new efficient adaptive data predistortion structures based on a Volterra system. The results are attractive due to the simplicity of the proposed structures: they are composed only of digital filters and memoryless nonlinear devices working at the symbol rate.

The paper is organized as follows: the reference model of the nonlinear link and its Volterra representation is reported in Section II and the analysis of the proposed compensation techniques is introduced in Section III, while Section IV shows some implementations. Section V is devoted

Paper approved by Peter J. Mc Lane, the Editor for Modulation Theory and Nonlinear Channels of IEEE Communications Society.
Manuscript received March 2, 1990; revised April 18, 1991; January 28, 1992.
This work was supported in part by MURST, the Italian Ministry of the University and Scientific Research.
S. Pupolin and G. Lazzarin are with the Dipartimento di Elettronica e Informatica, Università di Padova, via Gradenigo 6/A, 35131 Padua, Italy,
A. Sarti is with the Dipartimento di Elettronica e Informazione, Politecnico di Milano, Piazza L. Da Vinci 32, 20133 Milan, Italy.
IEEE Log Number 9400996.

to the adaptive technique proposed. The method for measuring the system performance is illustrated in Section VI, while in Section VII reports of simulation results and comparisons are given. Section VIII gives concluding remarks and comments on the applicability of the system and further research.

II. System Model

The system we are considering is represented in Fig. 1. The TX signal processing functions that are required to linearize the HPA are given, in this model, by the data predistorter and its adaptive parameter estimator, shown within the dashed box, while the analog predistorter box is included only for comparison. In Fig. 1 $\mathbb{Z}(T)$ is the discrete time domain with symbol period T, $\mathbb{R}$ is the continuous time domain and $\{a_n\}$ is a sequence of T-spaced complex symbols belonging to an L-QAM constellation so that both $Re\{a_n\}$ and $Im\{a_n\}$ take on values $\{\pm 1, \pm 3, \ldots, \pm(\sqrt{L}-1)\}$. $\{b_n\}$ is the sequence of T-spaced complex samples obtained by the nonlinear filtering of $\{a_n\}$. Driving the modulator with this sequence, the baseband equivalent signal driving the HPA is

$$x(t) = \sum_n b_n g(t - nT) \tag{1}$$

where $g(t)$ is the pulse shape of the modulator. We assume that $g(t)$ is a bandlimited function belonging to the class of the raised cosine rolloff function $C(f;\delta)$, that is

$$\frac{G(f)}{T} = [C(f;\delta)]^{\rho} \tag{2}$$

where $G(f)$ is the Fourier Transform of $g(t)$, δ is the rolloff factor $(0 < \delta < 1)$ and ρ is a real parameter $(0 < \rho \leq 1)$.

The radio channels of interest are narrowband, therefore the HPA can be treated as a nonlinear memoryless device [16], i.e. it performs a transformation $y = \Gamma(x)$, where Γ is a nonlinear complex function over a complex domain, chosen so that the maximum HPA output power $|y|^2 = P_{max}$ occurs when $|x|^2 = 1$. It follows that a general description of the HPA is given by the power series expansion of Γ:

$$y = \sum_{k=0}^{+\infty} \alpha_{2k+1} x(t) |x(t)|^{2k}, \tag{3}$$

where α_{2k+1} are the corresponding infinite series coefficients [17].

All the transformations that occur between the HPA and the detector, i.e. radio frequency filtering, radio channel and receive filter can be represented by a single baseband equivalent filter following the HPA in Fig. 1, whose impulse response is $h(t)$. We are assuming a fixed receive filter for which, in the absence of nonlinearity and selective fading, the overall link is a Nyquist channel. As a result, assuming $P_{max} = 1$, the receive filter must be designed so that

$$G(f)H(f) = TC(f;\delta) \tag{4}$$

where $H(f)$ is the Fourier Transform of $h(t)$.

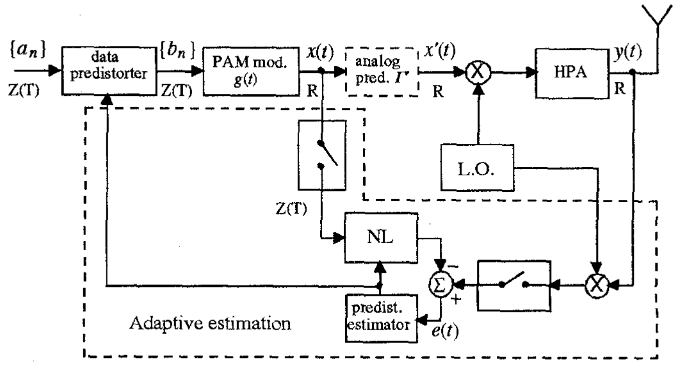

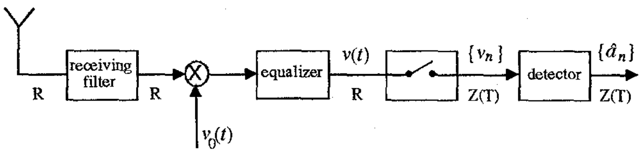

Fig. 1. Model of the nonlinear system.

The line-of-sight radio channel is represented during normal conditions as a filter with flat frequency response. In the presence of frequency selective fading this filter is time-varying so that, to compensate for ISI, an adaptive digital equalizer is placed after the fixed receive filter. Finally, we assume that the carrier reference is ideal, that the sampling in each symbol period occurs at the peak of the pulse and that the detector is composed of a set of fixed thresholds which would be optimal for a linear system with additive gaussian noise. In other words, the in-phase (quadrature) thresholds of an L-QAM constellation are set to detect $Re\{\alpha_n\}$ $(Im\{\alpha_n\})$ at $\{0, \pm 2, \pm 4, \ldots, \pm(\sqrt{L}-2)\}$. The discrete signal used to estimate the transmitted symbol sequence $\{a_n\}$ is $v_n + \eta_n$, where $\{\eta_n\}$ is a sequence of complex samples of noise.

III. Nonlinear Compensation

A. Analog Predistortion

To cope with the unwanted effects which stem from the nonlinear behavior of the HPA, we can insert an appropriate analog nonlinear device before the amplifier, as depicted in Fig. 1. The choice of the I/O relationship Γ' of this analog compensator depends on the available information on the HPA characteristic Γ. If the exact shape of Γ is known, then it is possible to implement the predistorter by selecting $\Gamma' = \Gamma^{-1}$ under appropriate constraints on the amplitude range of x, so that the cascade of the compensator and the amplifier behaves as linear $(y = x)$. We note that an analog predistorter could be implemented at baseband. To do this we must sample $x(t)$ at a rate multiple of $1/T$, process the samples with the Γ' characteristic and filter the output samples in order to drive the mixer with a continuous-time signal x'. The oversampling factor must be chosen in order to avoid aliasing on the x' signal, and must be at least equal to 2 for raised cosine pulse generation (comments of Appendix B will apply).

In practice we don't know exactly the HPA characteristic. On the other hand we can always implement a p^{th}-order predistorter

$$x'(t) = \sum_{k=0}^{(p-1)/2} \beta_{2k+1} x(t)|x(t)|^{2k} . \qquad (5a)$$

whose aim is to delete up to the p^{th}-order nonlinear terms of the power series expansion of Γ.

In general, the correction capability of the p^{th}-order analog predistorter is satisfactory for the AM-AM curve but is far from optimality as far as the AM-PM curve is concerned. We could compensate for the residual phase distortion by adding a polynomial AM-PM characteristic so that the I/O relationship turns out to be:

$$x' = \sum_{k=0}^{(p-1)/2} \beta_{2k+1} x|x|^{2k} \exp\left(j \sum_{i=2}^{p'} \phi_i |x|^i \right) . \qquad (5b)$$

B. Data Predistortion with Memory

The overall link that we have outlined in Section II is nonlinear with memory and may be represented by a discrete-time Volterra system Q having only odd order terms [17]. Its input-output relationship is given by:

$$v_n = \sum_{i=0}^{+\infty} \sum_{k_1 \cdots k_{2i+1}} b^\star_{k_1} \cdots b^\star_{k_i} b_{k_{i+1}} \cdots b_{k_{2i+1}}$$
$$q_{2i+1}(n-k_1, \ldots, n-k_{2i+1}) \qquad (6)$$

where v_n is the sequence of sampled data at the receiver,

$$q_{2i+1}(n_1, \ldots, n_{2i+1}) = \alpha_{2i+1} q'_{2i+1}(n_1, .., n_{2i+1}) \qquad (7)$$

and

$$q'_{2i+1}(n_1, \ldots, n_{2i+1}) =$$
$$\int_{-\infty}^{\infty} h(\tau) \prod_{j=1}^{i} g^\star(n_j T - \tau) \prod_{k=i+1}^{2i+1} g(n_k T - \tau) d\tau . \qquad (8)$$

The Volterra kernels (7) are completely specified whenever the HPA parameters α_{2i+1} and the pulse shape $g(t)$ are known. $h(t)$ is obtained by applying (4). A general approach to the design of a data predistorter with memory is based on the inversion of the above Volterra system [11].

Let b_n be the output of a discrete-time Volterra system P (with kernels p_i), driven by the source symbols a_n, and let $\{c_i\}$ be the kernels of the Volterra system given by the cascade of P and Q, namely:

$$v_n = \sum_{i=0}^{\infty} \sum_{k_1, \ldots, k_{2i+1}} a^\star_{k_1} \cdots a^\star_{k_i} a_{k_{i+1}} \cdots a_{k_{2i+1}}$$
$$c_{2i+1}(n-k_1, \ldots, n-k_{2i+1}). \qquad (9)$$

The discrete-time Volterra system P is a p^{th}-order inverse of Q if:

a) the first-order kernel of their cascade is a unit impulse

b) the other kernels up to the order p are zero.

In other words:

$$c_1(n) = \delta(n) = \begin{cases} 1 & n = 0 \\ 0 & n \neq 0 \end{cases} \qquad (10a)$$

$$c_{2i+1}(n_1, \ldots, n_i) = 0 , \qquad i = 1, 2, \ldots, (p-1)/2 \quad (10b)$$

In order to compute the kernels p_i of the predistorter, we write c_{2i+1} as follows:

$$c_{2i+1}(n_1, \ldots, n_{2i+1}) = \sum_{j=0}^{i} c^{(2j+1)}_{2i+1}(n_1, \ldots, n_{2i+1}) \qquad (11)$$

where $c^{(2j+1)}_{2i+1}$ represents the component of the $(2i+1)^{th}$-order kernel of the cascade of P and Q generated by the $(2j+1)^{th}$-order kernel of Q. We assume, without loss of generality, that the linear part of Q (i.e. the filter characterized by the first-order kernel) is equalized at the receiver, that is

$$q_1(n) = \alpha_1 \delta(n). \qquad (12)$$

Considering that

$$c^{(1)}_{2i+1}(n_1, \ldots, n_{2i+1}) = \sum_k q_1(k) p_{2i+1}(n_1 - k, \ldots, n_{2i+1} - k)$$
$$= \alpha_1 p_{2i+1}(n_1, \ldots, n_{2i+1}) \qquad (13)$$

the condition $(10a)$ gives

$$p_1(n) = \frac{1}{\alpha_1} \delta(n) , \qquad (14)$$

while the use of $(10b)$, (11) and (13) yields:

$$p_{2i+1}(n_1, \ldots, n_{2i+1}) = -\frac{1}{\alpha_1} \sum_{j=1}^{i} c^{(2j+1)}_{2i+1}(n_1, \ldots, n_{2i+1}) . \qquad (15)$$

After a tedious calculation, deferred to Appendix A, eq. (15) allows us to write the kernel p_{2i+1} recursively in terms of the kernels q_{2k+1}, $k \leq i$, of the Volterra system Q.

IV. Predistorter Structure

A. Implementation of the Predistorter

An efficient implementation of the p^{th}-order predistorter with memory must avoid a direct implementation of the Volterra system, as the complexity of the Volterra systems rapidly makes the system infeasible.

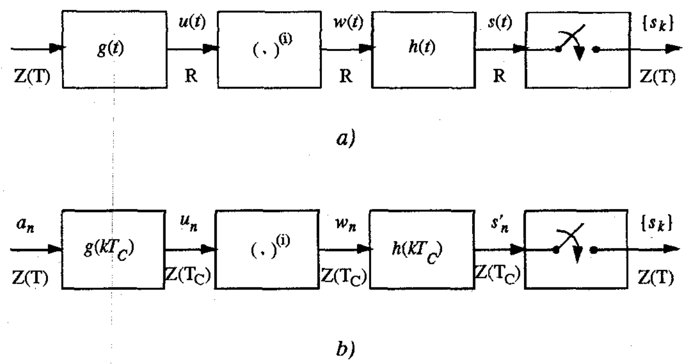

Fig. 2. Implementation of the $(2i+1)^{th}$-order kernel V_{2i+1} of the predistorter: analog *(a)* and digital *(b)* realizations.

Hereafter we present new efficient structures for the lower order predistorters ($p=3$ and $p=5$). We state the following theorem to aid in this task.

Theorem 1: *The system represented in Fig. 2(a) is equivalent to the discrete-time system of Fig. 2(b) under the following assumptions:*

a) *$g(t)$ is bandlimited to $B_g = \frac{1+d}{2T}$*

b) *$T_C = \frac{T}{M} \leq (2iB_g)^{-1}$, where M is an integer, and i is the order of the polynomial nonlinearity.*

The proof is given in Appendix B.

Remark. Theorem 1 shows how to simply implement the kernel V_{2i+1} of the predistorter in digital form. We note, in fact, the remarkable reduction in the complexity with respect to the direct implementation of V_{2i+1}.

1) Third-order structure: eq. (15) with $i=1$ gives the third-order kernel of the predistorter:

$$p_3(n_1,n_2,n_3) = -\frac{1}{\alpha_1} c_3^{(3)}(n_1,n_2,n_3). \tag{16}$$

The kernel $c_3^{(3)}$ equals the third-order kernel of the link q_3, apart from a scaling factor (see Appendix A). The resulting basic structure of the third-order predistorter is shown in Fig. 3, where $\beta_1 = 1/\alpha_1$, $\beta_3 = -\alpha_3/\alpha_1$ and the block V_3 is the Volterra system characterized by the kernel q'_3, which depends only on the filters $g(\cdot)$ and $h(\cdot)$ and it is independent of the HPA characteristic.

2) Fifth-order structure: the structure of the fifth-order predistorter is characterized by the third-order kernel (16) and by the fifth-order kernel defined by (15) with $i=2$:

$$p_5(n_1,\ldots,n_5) = -\frac{1}{\alpha_1}\left\{c_5^{(3)}(n_1,\ldots,n_5) + c_5^{(5)}(n_1,\ldots,n_5)\right\}. \tag{17}$$

It is easy to prove that the cascade of a third-order predistorter and the third-order kernel of the radio link generates both the kernels $c_3^{(3)}$ and $c_5^{(3)}$. This fact suggests us the basic scheme shown in Fig. 3 where β_1 and β_3 are defined as in the third-order case, $\beta_5 = -\alpha_5/\alpha_1$ and the realization of the system V_5 follows the same procedure outlined for V_3.

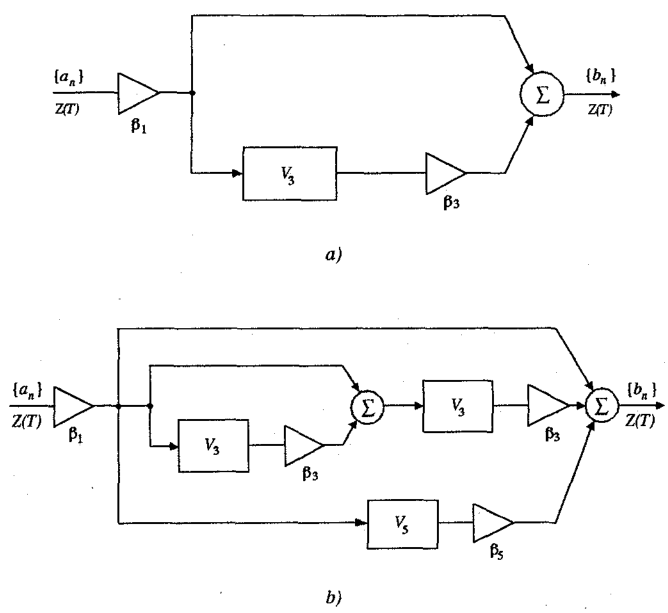

Fig. 3. Basic structure of the third-order and fifth-order predistorter.

3) Reduced fifth-order structure: the complexity of the basic scheme of the fifth-order predistorter can be reduced by expanding the nonlinear blocks V_3 and V_5 and redrawing the connections. We note that a digital interpolator g and a digital filter h can be shared by the branches of $c_3^{(3)}$ and $c_5^{(3)}$, and that, moreover, if the linear part of the third-order compensator picks-up and inserts the signal after the digital interpolators g, there is no alteration in the I/O relationship. These considerations lead to the scheme of Fig. 4(a).

A much simpler solution, whose complexity is close to that of the third-order, is achievable at the cost of a non-complete cancellation of the intermediate term $c_5^{(3)}$. The simplification arises by considering the digital interpolator g, which appears in the dashed box of Fig. 4(a), as composed by a digital interpolator with kernel $\delta(kT_C)$ followed by a digital filter with taps $g(kT_C)$ and by shifting this filter before the decimator. When $T_C = T/M$ with $M \geq 2$, this has the same effect as neglecting the dashed box of Fig. 4(a). Therefore we obtain the reduced scheme of Fig. 4(b) where:

$$\beta'_5 = -\frac{\alpha_5}{\alpha_1} + \frac{\alpha_3}{\alpha_1}\left\{2\frac{\alpha_3}{\alpha_1} + \frac{\alpha_3^\star}{\alpha_1^\star}\right\}. \tag{18}$$

A comparison between the system performance of the fifth-order predistorters will show the effectiveness of the reduced-complexity structure.

4) Realization: we write the I/O relationship of the scheme of Fig. 2(b), where the nonlinear device implements the complex function $w = f(u)$:

$$s_n = \sum_i h\left(nT - i\frac{T}{M}\right) f\left(\sum_j a_j g(i\frac{T}{M} - jT)\right) \tag{19}$$

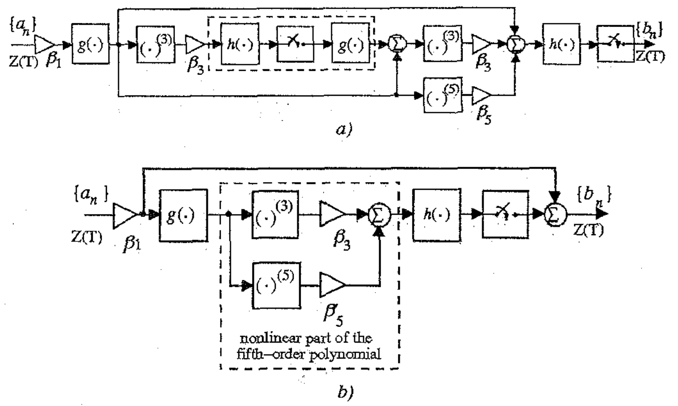

Fig. 4. Full fifth-order *(a)* and reduced fifth-order *(b)* predistorter.

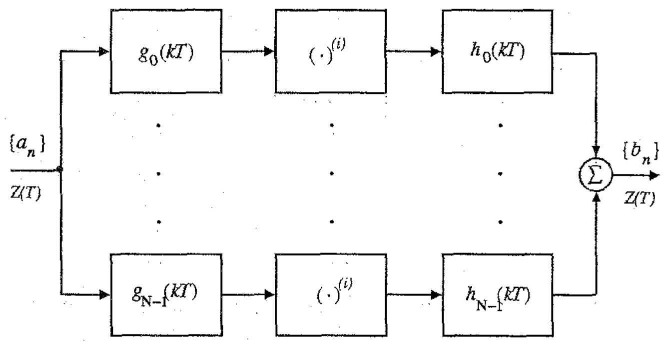

Fig. 5. Polyphase network for the systems V_{2i+1}.

By defining the two families of impulse responses:

$$h_m(k) = h\left(kT + m\frac{T}{M}\right) \qquad m = 0, 1, \ldots, M-1 \quad (20)$$
$$g_m(k) = g\left(kT - m\frac{T}{M}\right)$$

we obtain

$$s_n = \sum_{m=0}^{M-1} \sum_i h_m(n-i) f\left(\sum_j a_j g_m(i-j)\right), \quad (21)$$

which corresponds to the polyphase structure depicted in Fig. 5. This structure can be used to implement both systems, V_3 and V_5, in the scheme of Fig. 3 and can be easily extended to the systems sketched in Fig. 4. In this way the $(2i+1)^{th}$-order kernel is implemented by using M parallel filters working at symbol rate instead of just one filter working at M times the symbol rate.

B. Phase Compensation

The behavior of the p^{th}-order data predistorter with memory is similar to that of the analog predistorter. The compensated system, in particular, shows a considerable reduction of the nonlinear ISI, but it leaves a significant residual AM-PM distortion.

To cope with this problem we can insert before the predistorter with memory a zero-memory AM-PM predistorter (whose purpose is thus to compensate just for the AM-PM portion of the HPA distortion), or a polynomial AM-PM characteristic, as used in the analog predistorter.

V. Adaptive Estimation of Predistorter Parameters

A. Volterra Predistorter

One of the main advantages of the proposed schemes is that they require little information: only the shape of $G(f)$ and the HPA parameters α_1, α_3 and α_5 are needed. In fact, $G(f)$ is a known design choice, while the HPA coefficients are the only items necessary to estimate because their values depend on the operating point of the HPA, as well as being subjected to drift. A similar reasoning is valid for the AM-PM compensator.

HPA parameters. Considering that the coefficients to be estimated are slowly time-varying, without loss of generality, we assume their values to be fixed. If the sequence of T-spaced samples x_n and y_n of the input $x(t)$ and the output $y(t)$ of the HPA are available, it is possible to know the estimation error:

$$e_n = y'_n - y_n \quad (22)$$

where the measured output y_n and its estimated value y'_n can be expressed as follows

$$y_n = \mathbf{x}_n^T \underline{\alpha} + z_n \quad (23)$$

$$z_n(t) = \sum_{i \geq 3} \alpha_{2i+1} x_n |x_n|^{2i} \quad (24)$$

$$y'_n = \mathbf{x}_n^T \underline{\alpha}' \quad (25)$$

where $\mathbf{x}_n^T = [x_n, x_n|x_n|^2, x_n|x_n|^4]$, $\underline{\alpha}^T = [\alpha_1, \alpha_3, \alpha_5]$, $\underline{\alpha}'^T = [\alpha'_1, \alpha'_3, \alpha'_5]$, T denotes transposition, and z_n is the residual contribution of the HPA nonlinearities of seventh-order and greater. The estimation procedure for HPA parameters is given by the following

Theorem 2: *The optimum minimum square error (MSE) estimate of HPA vector parameters $\underline{\alpha}'_{opt}$ is given by:*

$$\underline{\alpha}'_{opt} = \mathbf{M}^{-1}\mathbf{c} + \underline{\alpha} \quad (26)$$

where $\mathbf{M}$ is the autocorrelation matrix of the vector $\mathbf{x}_n$,

$$\mathbf{M} = E[\mathbf{x}_n^\star \mathbf{x}_n^T] = \begin{bmatrix} m_x(2) & m_x(4) & m_x(6) \\ m_x(4) & m_x(6) & m_x(8) \\ m_x(6) & m_x(8) & m_x(10) \end{bmatrix}, \quad (27)$$

$\star$ denotes complex conjugate, $\mathbf{m}_x(i) = E[|\mathbf{x}_n|^i]$ is the i^{th}-order absolute moment of x_n, and

$$\mathbf{c} = \begin{pmatrix} \sum_{i=3}^{\infty} a_{2i+1} m_x(2i+2) \\ \sum_{i=3}^{\infty} a_{2i+1} m_x(2i+4) \\ \sum_{i=3}^{\infty} a_{2i+1} m_x(2i+6) \end{pmatrix} \quad (28)$$

The proof is reported in Appendix C.

A classic adaptive method for finding the optimum solution is the "stochastic gradient" algorithm whose update equation is

$$\underline{\alpha}'(n+1) = \underline{\alpha}'(n) - \Delta \mathbf{x}_n^\star e_n \tag{29}$$

where Δ is a constant whose value must be accurately selected in order to find a trade-off between stability and convergence speed of the algorithm. The resulting estimator follows a stochastic trajectory converging in a mean square sense to the solution of (26).

B. Phase compensation.

Compensation of the residual Phase distortion could be performed by using the memoryless predistortion algorithm proposed by Saleh and Salz [6], or by using an MSE estimator of phase parameters ϕ_i (see eq. (5.b)).

VI. Performance Evaluation

A. Definitions

The measure we consider for the system performance is the flat fade margin F [7], i.e. the signal reduction that can be sustained on the radio path before the bit error rate (BER) reaches a given performance threshold BER_0 (for the sake of concreteness we choose the value $BER_0 = 10^{-4}$). The flat fade margin is a function of the HPA working point, but it also depends on the operating conditions of the link. This is the reason we consider a relative measure of the flat fade margin F/F_{max}, where F_{max} is the maximum theoretical value of F corresponding to a given constellation, propagation path and maximum HPA power.

The HPA input backoff is defined as the reduction of the peak input power compared to the maximum value. Considering that the peak input power is

$$P_{in} = K^2 |g(0)|^2 \max_m \{|\gamma_m|^2\}, \tag{30}$$

where γ_m is the reference constellation, K is a scaling factor chosen for the HPA output to be maximum when $P_{in} = 1$. The input backoff thus corresponds to $10 \log P_{in}$. The primary output of the analysis is a set of curves of F/F_{max} versus HPA input backoff, from which we obtain the value P_{in}^0 of P_{in} which maximizes the flat fade margin. Such a value represents the best trade-off between the need of more signal distance and less nonlinear distortion.

B. Performance Measure

We assume that the in-phase and quadrature noise components in the rails of the detector input are additive, gaussian and uncorrelated with equal power σ_N^2. We then define the distance-to-noise ratio:

$$DNR = \frac{d^2}{\sigma_N^2}, \tag{31}$$

where d is the half-distance between the decision boundaries of the detector.

The BER is a decreasing monotonous function of the DNR and it assumes the value BER_0 when $DNR = DNR_0$. F is thus given by:

$$F = \frac{DNR}{DNR_0}. \tag{32}$$

The maximum value of F, F_{max}, can be achieved by considering the ideal case of linear HPA driven by rectangular pulses of duration T at the maximum power [8]. The relative flat fade margin is based on the measure of a pair of penalty factors which, multiplied together, give the amount by which F is lower than F_{max}:

$$\frac{F}{F_{max}} = \frac{1}{P_N P_C}. \tag{33}$$

The noise enhancement penalty P_N is related to the compensation of the HPA input backoff at the receiver and the nonideal filtering:

$$P_N^{-1} = \frac{1}{\max_m\{|\gamma_m|^2\}} \int_{-\infty}^{\infty} \left| \frac{C(f;\delta) H_{eq}(f)}{\frac{1}{T} G(g)} \right|^2 df \tag{34}$$

where $H_{eq}(f)$ is the frequency response of the equalizer (if used).

The cluster penalty P_C arises from the presence of nonlinear ISI at the detector and indicates the increase in the value of DNR required to achieve $BER = BER_0$. P_C is a function of P_{in} and can be expressed as follows:

$$P_C = \frac{DNR_0(P_{in})}{DNR_0(-\infty)}. \tag{35}$$

where $DNR_0(-\infty)$ is the value of the DNR_0 corresponding to the linear behavior of the HPA.

To evaluate the penalties (34) and (35), a Monte Carlo simulation program of the link of Fig. 1 has been carried out. The HPA has been modeled as a TWT amplifier according to the AM-AM and AM-PM characteristics described by Saleh [16]. The receiver thermal noise has been treated analytically for each sample at the input of the detector by computing the BER for specified σ_N^2 by using the complementary error function [18].

We have simulated the system in various operating conditions and for many values of the input back-off. For each value of P_{in}, a BER versus DNR curve has been drawn in order to evaluate $DNR_0(P_{in})$ and, by using eq. (35), the value of P_C. The corresponding frequency response of the adaptive equalizer has been used to compute the value of P_N according to eq. (34).

VII. Simulation Results

A. Comparisons of Compensation Techniques

The flat fade margin diagrams of the 64-QAM and 256-QAM systems are reported in Fig. 6. Eight different situations are considered: the solid curves represent the system behavior without AM-PM compensation and the dashed

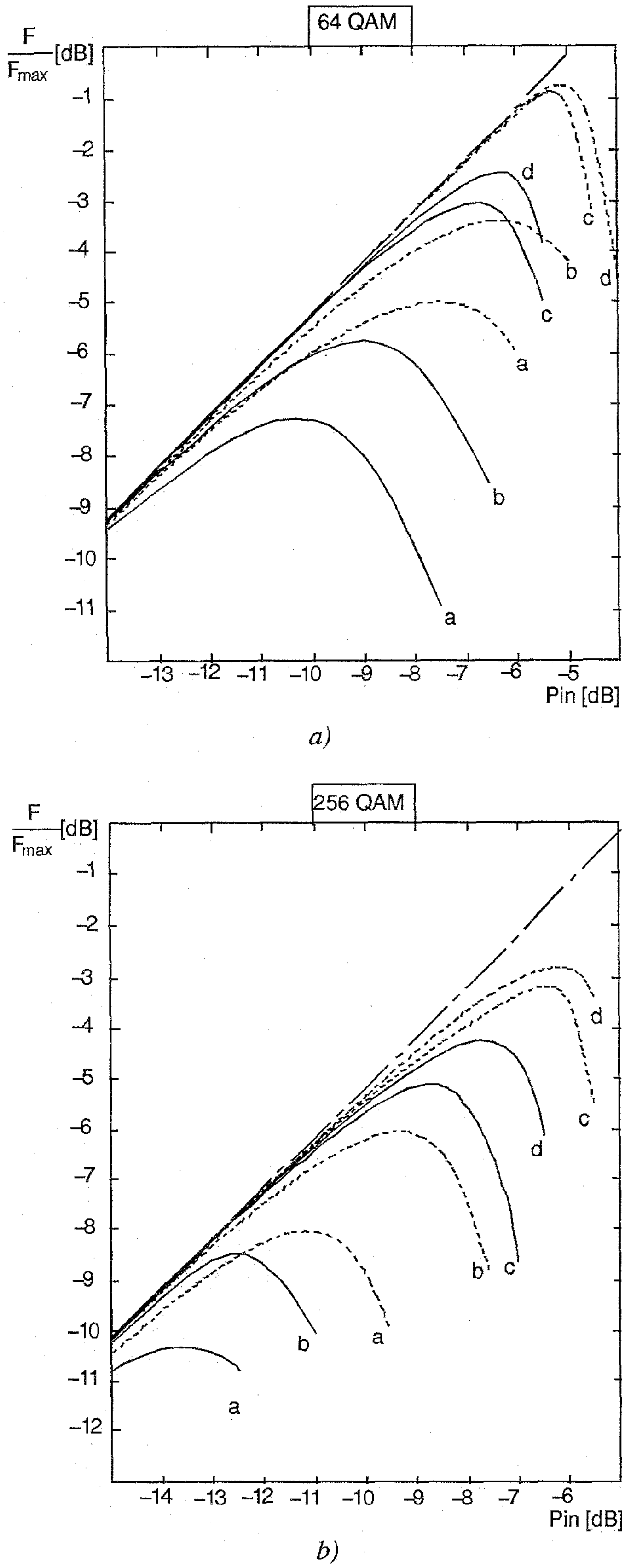

Fig. 6. Comparison of compensation strategies in 64-QAM *(a)* and 256-QAM *(b)* systems with (dashed lines) and without (solid lines) phase compensation. The curves are labeled as follows: a) no pred., b) 3^{rd}-order pred., c) reduced 5^{rd}-order pred., d) 5^{rd}-order pred.

TABLE I.
MAXIMUM F/F_{max} FOR DIFFERENT COMPENSATION STRATEGIES

		64-QAM		256-QAM	
predist.	*phase comp.*	$\frac{F_p}{F_{max}}$ $[dB]$	*Gain* $[dB]$	$\frac{F_p}{F_{max}}$ $[dB]$	*Gain* $[dB]$
no predist.	*no*	-7.29	0	-10.25	0
	yes	-5.10	2.19	-8.06	1.6
3^{rd} *order*	*no*	-5.82	1.47	-8.59	1.66
	yes	-3.42	3.87	-6.10	4.15
reduced 5^{th}*-ord.*	*no*	-3.03	4.26	-5.15	5.10
	yes	-1.26	6.03	-3.24	7.01
5^{th} *order*	*no*	-2.46	4.83	-4.21	6.04
	yes	-0.97	6.32	-2.84	7.41
memoryless 5^{th}*-ord.*		-1.56	5.73	-5.30	4.95

curves represent the performance improvement due to a phase correction of $p' = 2$. The results are labeled as follows: a) no predistortion, b) third-order predistortion, c) reduced fifth-order predistortion, and d) full fifth-order predistortion. We refer to a standard situation in which $G(f)$ is a root-cosine rolloff function ($\rho = 0.5$) with rolloff factor $\delta = 0.5$ and $G(f)H(f)$ is a full cosine rolloff function with the same rolloff factor. In each case an adaptive linear equalizer is used [8]. The maximum values F_p/F_{max} of the relative flat fade margins corresponding to the curves of Fig. 6 are gathered in Table I, where the performance gains with respect to the uncompensated case are reported as well.

We note that the gain obtained by using the third-order predistorter, even with quadratic phase compensation, is quite small and lower than the gain due to a single memoryless predistorter. In fact, the main limit of a third-order predistorter is the residual warping of the constellation at the detector rather than the size of the clusters due to nonlinear ISI.

A full fifth order predistortion with quadratic phase compensation produced another $2.5dB$ improvement for 64-QAM and $3.3dB$ for 256-QAM. The reduced fifth order predistorter has a performance only $0.4dB$ worse than the full fifth order predistorter with a much lower complexity. We note that for 64-QAM the memoryless predistorter has a performance close to the one proposed. This is due to the fact that performance degradation is due more to the residual distortion rather than to nonlinear ISI. For the 256-QAM we note an improvement of over $2dB$ in performance for the proposed predistorter. This is mainly due to the reduction of nonlinear ISI.

The best results have been achieved using both full fifth-order predistorter and phase compensator. The relative flat fade margin for a 64-QAM system reaches the value $F_p/F_{max} = -0.97dB$ and for a 256-QAM system we have $F_p/F_{max} = -2.84dB$. We notice that these values are close to those of a linear QAM system with saturation at P_{max} with the same pulse shaping, where we have $F_p/F_{max} =$

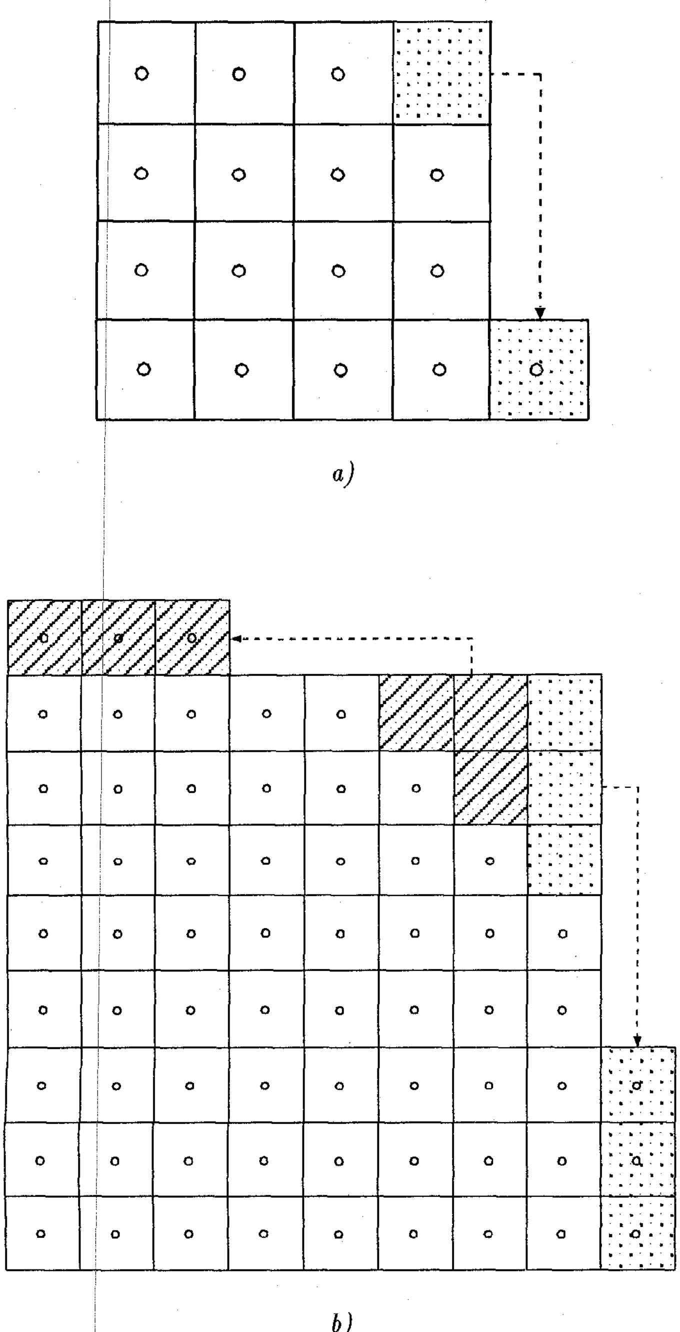

Fig. 7. Modified 64-QAM *(a)* and 256-QAM *(b)* constellations.

$-0.65dB$ for a 64-QAM system and $F_p/F_{max} = -1.13dB$ for a 256-QAM system.

A further improvement is achievable by modifying the reference constellation in order to reach a higher d^2/P_{max}, which causes P_N to decrease. For example, the modified 64-QAM (256-QAM) constellation shown in Fig. 7 causes a reduction of P_N of $0.77dB$ ($1.56dB$). We have verified by simulation that, apart from a few hundredths of dB, the use of a modified constellation does not affect the cluster penalty. In other words, the reduction of the noise penalty gives rise to an equal increase of the the flat fade margin.

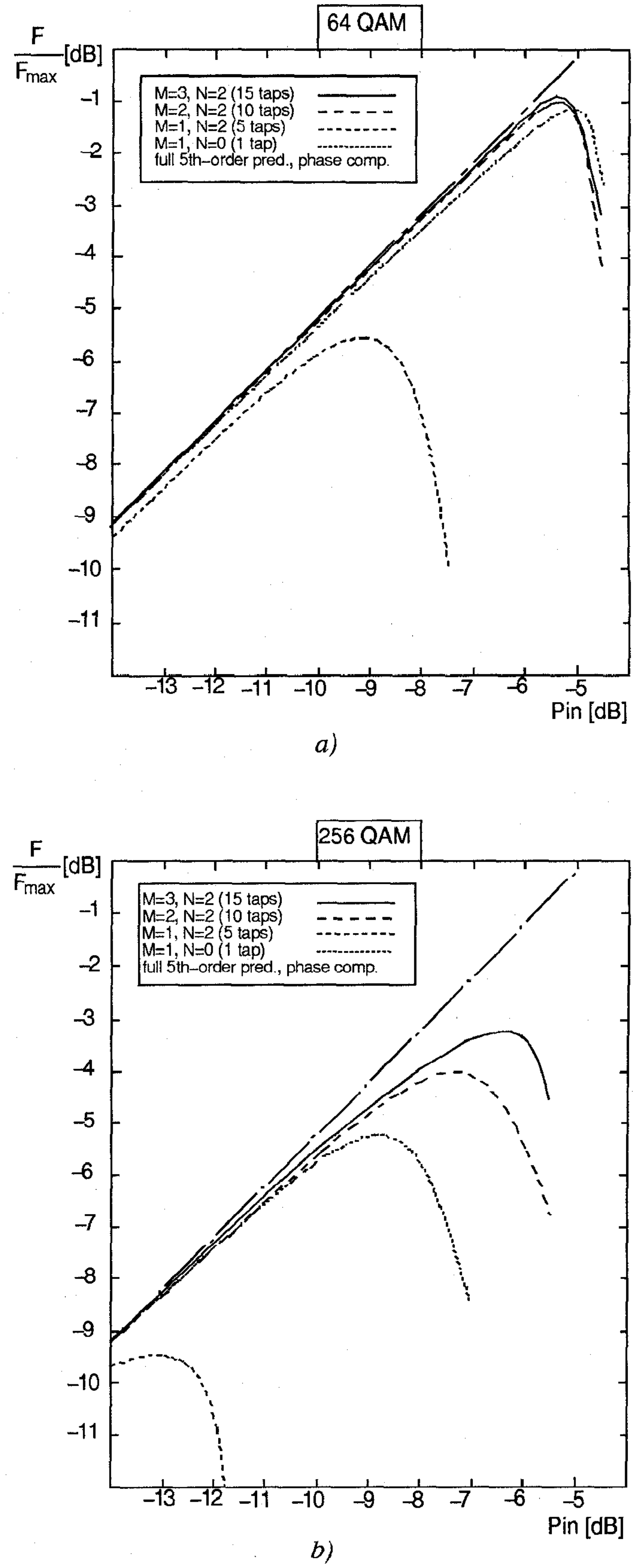

Fig. 8. Comparison of F/F_{max} versus P_{in} for different values of M and N in 64-QAM *(a)* and 256-QAM *(b)* systems with full fifth-order predistortion and phase compensation.

B. Complexity Reduction

A crucial aspect of the design of a predistorter is the minimization of its complexity without affecting its performance.

To find a good trade-off between complexity and effectiveness of the compensation strategy we have computed, through simulation, the flat fade margin diagrams corresponding to predistorter configurations which differ in their complexity. The complexity is measured in terms of the oversampling factor M, corresponding to the number of branches of the parallel structure of Fig. 5, and of the number of taps $2N+1$ of each filter appearing in the same scheme. We found that the 64-QAM and 256-QAM systems behave differently when M and/or N are reduced. Fig. 8a shows the performance of a 64-QAM system with a full fifth-order predistorter and a phase compensator when M and N fall below the thresholds $M = 3$ and $N = 2$. We notice that the flat fade margin curve which corresponds to the use of a fifth-order memoryless predistorter and a quadratic phase compensator ($M = 1$, $N = 0$) is very close to the one corresponding to $M = 3$ and $N = 2$. This fact confirms that the clustering effect is not the main source of impairment for a 64-QAM system as a mere correction of the cluster positions improves the performance almost as much as a nonlinear predistorter with memory of the same order. On the other hand, the choice $M = 1$, $N = 2$ leads to a large reduction of the flat fade margin. Roughly speaking this means that "no memory" is better than a "bad memory".

In the case of a 256-QAM system the situation, shown in Fig. 8b, is quite different. The degradation that occurs when a fifth-order memoryless predistorter with phase compensation is used is heavy because the high number of levels increases the system sensitivity to the nonlinear ISI. On the other hand, if the predistorter works with $M = 2$ and $N = 2$ (10 taps over $\mathbb{Z}(T/2)$), then the performance degradation results as being very mild (about $1dB$), even if the conditions of the sampling theorem are not strictly met.

C. Filter Design

The above discussions refer to a standard situation in which $G(f)/T = C(f;\delta)^{\rho}$ and $H(f) = C(f;\delta)^{1-\rho}$, with $\rho = 0.5$ e $\delta = 1/2$. Two further solutions have been considered: the former selects $\frac{1}{T}G(f)H(f) = C(f;0.5)$ and $\frac{1}{T}G(f) = C(f;\delta_1)$ with $\delta_1 \geq 0.5$, the latter selects $\frac{1}{T}G(f) = C(f;0.5)^{2/3}$ and $H(f) = C(f;0.5)^{1/3}$, which represents the optimal pulse shaping for linear peak-power-limited HPA.

System performance for the former choice has been obtained for a 64-QAM system with a reduced fifth-order predistorter and a phase compensator. The results, reported in Table II for $\delta_1 = 0.5$, $\delta_1 = 0.75$ and $\delta_1 = 1$, are notably worse than in the standard situation because of the increase of the noise penalty.

We have compared the latter strategy with the standard filter choice for both 64 and 256-QAM systems. Also in this case the system performance results as being worse than that obtained with the standard filter choice, but the loss is lower than with the former non-standard choice. We note that the performance loss for the 64-QAM is practically all due to the noise penalty, while the 256-QAM looses more than 1dB just for the cluster penalty.

TABLE II.
MAXIMUM F/F_{max} VS. TRANSMITTER SHAPING FILTER AND SELECTIVE FADING WITH REDUCED 5^{th}-ORDER PREDISTORTER AND PHASE COMPENSATION

	Fading $[dB]$	δ_1	ρ	$\frac{F_p}{F_{max}}$ $[dB]$	*Gain* $[dB]$	P_N $[dB]$
64 QAM	*no*	0.5	1/2	-1.26	0	0
		0.5	1	-3.79	-2.53	-1.76
		0.75	1	-2.86	-1.60	-1.20
		1	1	-3.03	-1.77	-1.54
		0.5	2/3	-1.66	-0.40	-0.334
256 QAM	*no*	0.5	1/2	-3.24	0	0
		0.5	2/3	-4.92	-1.68	-0.334
64 QAM	-14	0.5	1/2	-17.16	-15.90	-3.27
256 QAM	-14	0.5	1/2	-21.83	-18.59	-3.18

D. Presence of Fading

System performance has been evaluated also in the presence of selective fading for both 64-QAM and 256-QAM systems. The filters $G(f)$ and $H(f)$ have been chosen to be equal to the standard case and the fading has been described with the Rummler's three-paths model [19] with a maximum fade of $14dB$ occuring exactly at the center of the band. The relative delay τ/T has been chosen to be equal to the 0.147 for the 64-QAM, and equal to 0.110 for the 256-QAM, corresponding to a $140Mbit/s$ digital system. In both cases the adaptive equalizer that we used to combat the fading effects has seven taps.

The simulation results, reported in Table II, show that the interaction between nonlinearity and fading gives rise to a performance degradation which is worse than that due to a flat attenuation of $14dB$. This phenomenon is due to the presence of residual ISI that the adaptive equalizer is unable to cancel when the selective fading occurs.

E. Transmitted Signal Spectrum

The spectrum of the transmitted signal has been computed in order to observe the spreading produced by the HPA considering the uncompensated as well as the compensated system (Fig. 9). We notice that in correspondence to the optimum system performance the transmitted spectrum of both compensated and uncompensated systems is nearly the same. The motivation of this unexpected behavior is presently unknown.

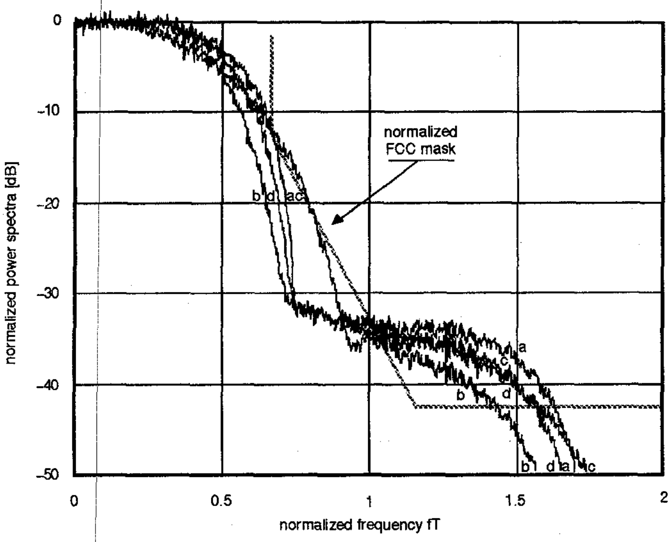

Fig. 9. Normalized power spectral density of the signal after the HPA.
a) $G(f) = C(f;0.5)^{1/2}$
b) $G(f) = C(f;0.5)$
c) $G(f) = C(f;1)$
d) $G(f) = C(f;0.5)^{2/3}$

VIII. Conclusions

New ways to compensate for the nonlinearities introduced by the power amplifier in the digital radio links have been developed. We have verified the effectiveness of the proposed solutions by showing that it is possible to linearize the channel almost completely without the need of overly costly circuits. We have also controlled the robustness of the estimator technique used to make the system adaptive and the behavior of the compensators in the presence of selective fading. Finally, several realistic operating conditions have been considered for a comparative analysis.

The proposed solutions differ from each other in effectiveness and complexity. The best results are achievable with the full fifth-order predistorter with phase compensation and modified constellation. Perhaps the best trade-off between complexity and performance is represented by the reduced fifth-order predistorter with phase compensation and modified constellation. We have shown that the predistorter is robust and that it brings the system performance close to the optimum value.

A final rough comparison with the analog predistorter is mandatory. The present technology enables us to insert the analog predistorter at baseband, just between the baseband filtering and IF mixers, instead of inserting it at IF as done in the past. We note the following drawbacks of the use of the analog predistorter:
i) it requires the sampling of the baseband signal at a rate which is a multiple of the baud rate in order to avoid aliasing;
ii) it requires A/D conversion with a large number of bits per sample in order to reduce the quantization noise;
iii) the nonlinear transformation is as complex as that of the predistorter;
iv) an analog filter is required to recover the analog signal before the mixer.

The complexity of this system is of the same order as that of the data predistorter proposed in this paper. However, we note that the data predistorter presented in this paper could be used in working systems by inserting it just before the PAM modulators, while the analog predistorter requires a re-design of the system to be placed in front of the IF mixers.

More attention has been recently devoted to the design of digital systems with a narrower bandwidth ($\rho = 0.2 - 0.3$). In this case the nonlinear ISI plays a more relevant role in the system performance as the ratio between the transmitted signal peak and the transmitted pulse peak is higher than in the proposed case. This could change the conclusion about the best filter design choice given here.

Finally, further research should be done to find a TX predistortion strategy which is able to reduce the signal spectrum sidelobes to meet the FCC requirements without the need of an RF filter, which the strategy here presented failed to reach.

Appendix A
Computation of the Kernels of the Predistorter

The complete expressions of the partial third- and fifth-order kernels of the overall link are:

$$c_3^{(3)}(n_1,n_2,n_3) = \sum_{k_1k_2k_3} q_3(k_1,k_2,k_3)$$
$$p_1^\star(n_1-k_1)p_1(n_2-k_2)p_1(n_3-k_3) \qquad (A.1)$$

$$c_5^{(1)}(n_1,\ldots,n_5) = \sum_k q_1(k)p_5(n_1-k,\ldots,n_5-k) \quad (A.2)$$

$$c_5^{(3)}(n_1,\ldots,n_5) = \sum_{k_1k_2k_3} q_3(k_1,k_2,k_3)$$
$$\{p_1^\star(n_1-k_1)p_1(n_2-k_2)p_3(n_3-k_3,n_4-k_3,n_5-k_3)$$
$$+p_1^\star(n_1-k_1)p_3(n_2-k_2,n_3-k_2,n_4-k_2)p_1(n_5-k_3)$$
$$+\,p_3^\star(n_1-k_1,n_2-k_1,n_3-k_1)p_1(n_4-k_2)p_1(n_5-k_3)\} \qquad (A.3)$$

$$c_5^{(5)}(n_1,\ldots,n_5) = \sum_{k_1\cdots k_5} q_5(k_1,\cdots,k_5)p_1^\star(n_1-k_1)$$
$$p_1^\star(n_2-k_2)p_1(n_3-k_3)p_1(n_4-k_4)p_1(n_5-k_5) \qquad (A.4)$$

Recalling eqs. (7), (12), (14) and (15) we obtain:

$$c_3^{(3)}(n_1,n_2,n_3) = \frac{\alpha_3}{\alpha_1|\alpha_1|^2}q_3'(n_1,n_2,n_3) \qquad (A.5)$$

$$p_3(n_1,n_2,n_3) = -\frac{\alpha_3}{\alpha_1|\alpha_1|^2}q_3'(n_1,n_2,n_3) \qquad (A.6)$$

$$c_5^{(5)}(n_1,\ldots,n_5) = \frac{\alpha_5}{\alpha_1|\alpha_1|^4}q_5'(n_1,\ldots,n_5) \qquad (A.7)$$

$$c_5^{(3)}(n_1,\ldots,n_5) = -\tfrac{\alpha_3}{\alpha_1}$$

$$\left\{ \frac{\alpha_3}{\alpha_1|\alpha_1|^4} \sum_m q_3'(n_1,n_2,m) q_3'(n_3-m,n_4-m,n_5-m) \right.$$

$$+ \frac{\alpha_3}{\alpha_1|\alpha_1|^4} \sum_m q_3'(n_1,m,n_5)) q_3'(n_2-m,n_3-m,n_4-m)$$

$$\left. + \frac{\alpha_3^\star}{\alpha_1^\star|\alpha_1|^4} \sum_m q_3'(m,n_4,n_5) q_3'(n_1-m,n_2-m,n_3-m) \right\} \qquad (A.8)$$

$$p_5(n_1,\ldots,n_5) = -\frac{1}{\alpha_1} c_5^{(3)}(n_1,\ldots,n_5) + c_5^{(5)}(n_1,\ldots,n_5) \qquad (A.9)$$

Appendix B

Proof of Theorem 1

The scheme of Fig. 2(a) has a single $(2i+1)^{th}$-order kernel given by the expression (8). Its Fourier transform can be expressed as follows:

$$Q'_{2i+1}(f_1,\ldots,f_{2i+1}) =$$

$$\sum_{k_1\cdots k_{2i+1}} H\left(\sum_{j=1}^{2i+1}\left(f_j - \frac{k_j}{T}\right)\right) \prod_{j=1}^{2i+1} G\left(f_j - \frac{k_j}{T}\right) \qquad (B.1)$$

Notice that the signals u, w and s are bandlimited to $B_u = B_g$, $B_w \le iB_g$ (see [20]) and $B_s = \min\{B_w, B_h\}$, we can obtain $w(t)$ from its samples taken at a rate $1/T_C \ge 2B_w$. If we choose T_C to be a submultiple of T, i.e. $T_C = T/M$ we can implement $g(t)$ as a digital filter (Fig. 2(b)).

Finally, for the system of Fig. 2(b) we have:

$$Q_i(f_1,\ldots,f_{2i+1}) = \sum_{k_1\cdots k_{2i+1}} \sum_k H\left(\sum_{j=1}^{2i+1}\left(f_j - \frac{k_j}{T}\right) - \frac{kM}{T}\right)$$

$$\prod_{j=1}^{2i+1} G\left(f_j - \frac{kj}{T}\right) \qquad (B.2)$$

From the assumptions **(a)** and **(b)**, it follows that the summation on k is non-zero only for $k=0$, thus the expressions $(B.1)$ and $(B.2)$ are equal.

Appendix C

Proof of Theorem 2

The MSE is given by:

$$E[|e_n|^2] = E[(\mathbf{x}_n^T(\underline{\alpha}' - \underline{\alpha}) - z_n)^\star(\mathbf{x}_n^T(\underline{\alpha}' - \underline{\alpha}) - z_n)] \, , \quad (C.1)$$

where E denotes "expectation" and "$\star$" denotes a complex conjugate. The vector minimizing the MSE is the solution of the equation

$$E[2\mathbf{x}_n^\star e_n] = 0 \, . \qquad (C.2)$$

The use of eqs. (22), (23), (24) and (25) in $(C.2)$ yields:

$$E[\mathbf{x}_n^\star(\mathbf{x}_n^T(\underline{\alpha}' - \underline{\alpha}) - z_n)] = 0 \qquad (C.3)$$

By using definitions (27) and (28), $(C.3)$ becomes as follows:

$$\mathbf{M}(\underline{\alpha}' - \underline{\alpha}) = \mathbf{c} \, . \qquad (C.4)$$

Finally, the optimum set of coefficients is given by (26) as long as M is invertible, which is always true because M is an autocorrelation matrix.

References

[1] M.F. Mesiya, P.J. Mc Lane, L.L. Campbell, *Maximum likelihood receiver for carrier-modulated data transmission systems*, IEEE Trans. Commun., Vol. COM-32, pp. 624-636, May 1973.

[2] W. Van Etten, F. Van Vugt, *Maximum likelihood receivers for data sequences transmitted over nonlinear channels*, A.E.T., Vol. 34, pp. 216-223, 1980.

[3] D.D. Falconer, *Adaptive equalization of channel nonlinearities in QAM data transmission systems*, Bell Syst. Tech. J., Vol. 57, n. 7, pp. 2589-2611, Sept. 1978.

[4] S. Benedetto, E. Biglieri, *Nonlinear equalization of digital satellite channels*, IEEE J. Select. Areas Commun., Vol. SAC-1, pp. 57-62, Jan. 1983.

[5] E. Biglieri, A. Gersho, R.D. Gitlin, T.L. Lim, *Adaptive cancellation of nonlinear interference for voiceband data transmission*, IEEE J. Select. Areas Commun., Vol. SAC-2, pp. 765-777, Sept. 1984.

[6] A.A.M. Saleh, J. Salz, *Adaptive linearization of power amplifiers in digital radio systems*, Bell Syst. Tech. J., Vol. 62, No. 4, pp. 1019-1033, Apr. 1983.

[7] S. Pupolin, L.J. Greenstein, *Digital radio performance when the transmitter spectral shaping follows the power amplifier*, IEEE Trans. Commun., Vol. COM-35, pp. 261-266, No. 3, Mar. 1987.

[8] S. Pupolin, L.J. Greenstein, *Performance analysis of digital radio links with nonlinear transmit amplifiers*, IEEE J. Select. Areas Commun., Vol. SAC-5, pp. 534-546, No. 3, Apr. 1987.

[9] J. Namiki, *An automatically controlled predistorter for multilevel quadrature amplitude modulation*, IEEE Trans. Commun., Vol. COM-31, pp. 707-712, No. 5, May 1983.

[10] M. Nannicini, P. Magni, F. Oggioni, *Temperature controlled predistortion circuits for 64-QAM microwave power amplifiers*, Proceedings of IEEE Microwave Symp., June 1985, S. Louis, MO.

[11] E. Biglieri, S. Barberis, M. Catena: *Analysis and compensation of nonlinearities in digital trasmission systems.* "IEEE J. Select. Areas Commun.", Vol. SAC-6, Jan 1988, No. 1, pp. 42-51.

[12] G. Karam, H. Sari, *Analysis of predistortion, equalization and ISI cancellation techniques in digital radio systems with nonlinear transmit amplifier*, IEEE Trans. Commun., Vol. COM-37, pp. 1243-1250, No. 12, Dec. 1989.

[13] S. Pupolin, A. Sarti, H. Fu: *Performance analysis of digital radio links with nonlinear transmit amplifier and data predistorter with memory.* IEEE International Communication Conference 1989, Boston, MA, June 1989.

[14] G. Karam, H. Sari, *Improved data predistortion using intersymbol interpolation*, Proceedings of the International Communications Conference 1989, June 1989, Boston, MA.

[15] G. Karam, H. Sari, *Implementation and performance of data predistortion with memory in digital microwave radio*, in Proceedings of GLOBECOM 1989, Nov. 1989, Dallas, TX.

[16] A.A.M. Saleh: *Frequency-independent and frequency-dependent nonlinear models of TWT amplifiers.* "IEEE Trans. Commun.", Vol. COM-29, Nov. 1981, No. 11, pp. 1715-1720.

[17] S. Benedetto, E. Biglieri, R. Daffara: *Modeling and performance evaluation of nonlinear satellite links - a Volterra series approach.* "IEEE Trans. Aerosp. El. Syst.", Vol. AES-15, Jul. 1979, No. 4.

[18] M.J. Jeruchim, *Techniques for estimating the bit error rate in the simulation of digital communication systems*, IEEE J. Select. Areas Commun., Vol. SAC-2, pp. 153-170, No. 1, Jan. 1984.

[19] C.W. Lundgren, W.D. Rummler, *Digital radio outage due to selective fading. Observation vs. prediction from laboratory simulation*, Bell Syst. Tech. J., Vol. 58, No. 5, pp. 1073-1100, May-June 1979.

[20] G. Bilardi, S. Pupolin, *Spectral analysis of the powers of a PAM digital signal,* AEI Alta Frequenza, Vol. 53, No. 2, pp. 70-76, Mar.-Apr. 1984.

Giovanni Lazzarin was born in Padova, Italy, on May 3, 1957. He received the Laurea degree in Electronic Engineering from the University of Padova, Padua, Italy, in 1989. From 1984 to 1990 he was with ASST, Italian State Telephone Agency. Since 1990 he has been with CERVED, Padua, Italy, where his area of interest is videotex systems and remote data base access through public data network.

Silvano Pupolin (S'68, M'71, SM'83) was born in Venice, Italy, on February 17, 1947. He received the Laurea degree in Electronic Engineering from the University of Padova, Padua, Italy, in 1970. He then joined the Department of Electronics and Informatics of the University of Padova, where he currently is a Full Professor of Electrical Communications. Since 1976 he has also been a consultant of Telettra SpA in Milan, Italy. In 1985 he spent the summer in Holmdel, NJ, doing research for the AT&T Bell Laboratories. He is actively engaged in researches on digital communications, including coherent optical communications, digital radio and spread spectrum systems, and packet radio networks. Mr. Pupolin is a Senior Member of IEEE and Member of AEI.

Augusto Sarti (S'86-M'93) was born in Rovigo, Italy, in 1963. He received the "laurea" degree (Summa cum Laude) in Electrical Engineering in 1988 and a doctoral degree in Electronics and Information Engineering in 1993, both from the University of Padova, Padua, Italy.

He worked for one year for the Italian National Research Council, doing research on optical communications. He then spent two years doing research work on nonlinear system theory at the University of California, Berkeley. Dr. Sarti is currently an Assistant Professor at the Politecnico di Milano, Milan, Italy and his research interests are on digital communications and nonlinear system theory.